Journal of Engineering and Applied Sciences 12 (Special Issue 10): 8900-8908, 2017
ISSN: 1816-949X

An Analysis on the Improvement of Fluidity According to the Configuration Change of Automotive Exhaust Port

[1]Kye-Kwang Choi and [2]Jae-Ung Cho
[1]Department of Metal Mold Design Engineering,
[2]Division of Mechanical and Automotive Engineering, Graduate School, Kongju National University,
1223-24 Cheonan Daero, Seobuk-gu, 31080 Cheonan-si, Chungnam, Korea

Abstract: Although, many technologies are being developed for the increase of vehicle's engine efficiency, these are based on smooth air flow for intake and exhaust. In this study, the flow situations were derived through a simulation analysis to secure basic data for the improvement of flow as a function of diameter and curvature of exhaust port. Analysis is carried out with the diameters of exhaust port into 12 and 20 mm and flow characteristics under diversified environments are evaluated as a function of height of valve lift. To simulate discharge characteristics of the exhaust gas inside combustion chamber, differences in the pressure were set up between combustion chamber interior and atmosphere and environments upon discharge of the air of a high temperature to outside were derived through a simulation analysis. When the diameter of exhaust port was increased, the pressure difference between inside and outside of the combustion chamber could be seen to be increased by 2.4% for the diameter of 20 mm compared with 12 mm while the inside flow rate could be affirmed to be higher by 0.5% for the diameter of 12 mm. However, as higher occurrence of Eddy currents for complete discharge of residual exhaust gas inside could be observed for the diameter of 20 mm, correlations in the combustion chamber as a function of diameter and curvature of the exhaust port could be identified. By providing the basic data for design of exhaust port to discharge exhaust gas based on the present study results, it is considered that a contribution can be made to optimization design.

Key words: Vehicle exhaust port, diameter, flow analysis, pressure, improvement, combustion, pressure

INTRODUCTION

Although, domestic and overseas vehicles are gradually being replaced by hybrid automobiles little by little, the needs for internal combustion engines are nevertheless still high. As the interests in exhaust gas are being globally enhanced and regulations on exhaust gas are being emerged as an important issue for each country, efforts to reduce discharged gas are continued. Many technologies for this purpose are being developed, turbocharger and GDI, VVT, CVVL, etc., may be considered as the examples. However, for such technologies to be applied, smooth intake and exhaust should be presupposed. The easiest method for smooth intake and exhaust is to have smooth flow of air inside the engine. While flow characteristics of the intake system are very important in the volumetric efficiency aspect counted as an important variable of engines having smooth discharge of exhaust gas is preemptive. If the exhaust gas cannot exit the combustion chamber smoothly after combustion, the volume of air upon intake has to be reduced as a sufficient pressure difference is not produced. Therefore, the efficiency degradation due to flow degradation of the exhaust gas becomes unavoidable before flow in the intake system to avoid such efficiency degradation. Therefore, in this study, a flow analysis was conducted by varying the shape of exhaust port and the amount of valve lift and shapes for efficient exhaust port will be derived by identification of flow performance as a function of diameter and shape of such exhaust port as well as position of the valve lift (Rotaru, 2017; Sourdis, 2015; Shaidarova *et al*., 2017; Han *et al*., 2017; Eckhardt, 2017; Creamers, 2017; Kim *et al*., 2017). On the basis of such study results, it is considered that performance factors for design of the exhaust port can be presented and their use as the basic data for increase in combustion efficiency for vehicles is possible.

MATERIALS AND METHODS

Research model: Figure 1 represents 3D modelling of an actual item for flow performance and the model was configured with focus on the diameter of exhaust port for the errors which can occur in the analysis and for the

Corresponding Author: Jae-Ung Cho, Division of Mechanical and Automotive Engineering, Graduate School, Kongju National University, 1223-24 Cheonan Daero, Seobuk-gu, 31080, Cheonan-si, Chungnam, Korea

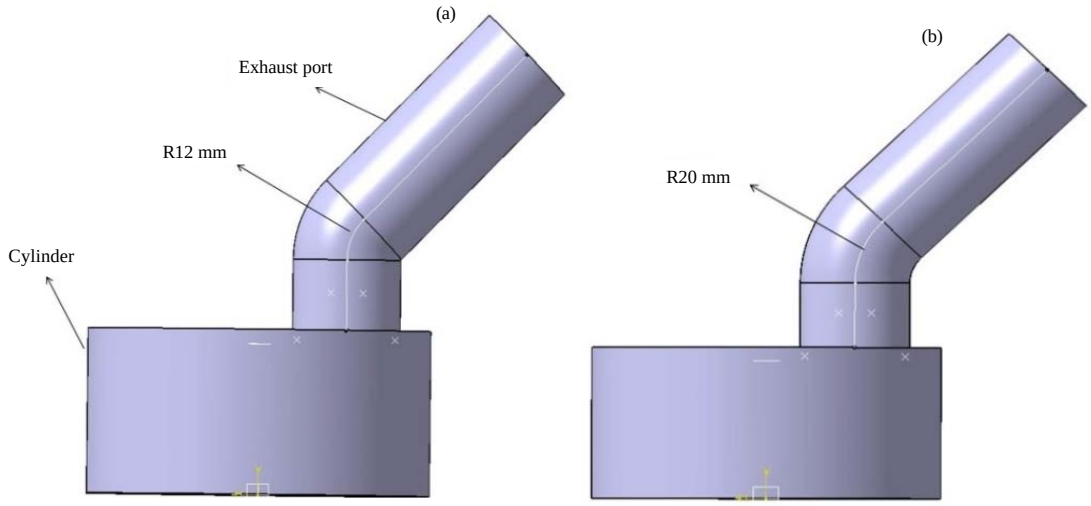

Fig. 1: Analysis model: a) Model 1 (R = 12 mm) and b) Model 2 (R = 20 mm)

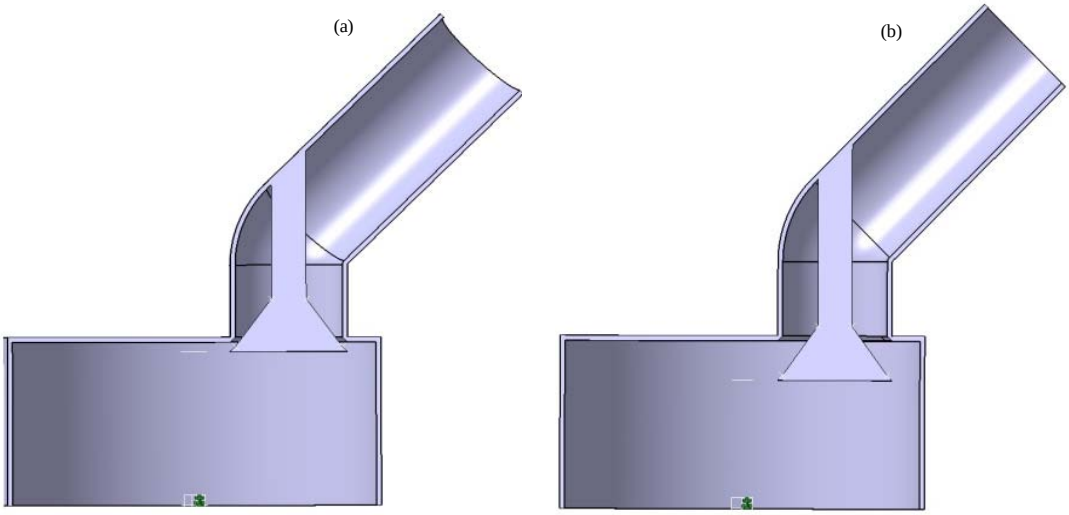

Fig. 2: Schematic diagrams for opening of valve lift in analysis model: a) Case 1 (opening and closing 2 mm) and b) Case 2 (opening and closing 8 mm)

Table 1: Geometrical parameters of analyzed ports

Curvature (mm)	Valve seat diameter (mm)	Valve lift (mm)
12	23.5	2, 4, 6, 8
20	23.5	2, 4, 6, 8

accuracy of values. Diameters of the exhaust port were 12 and 20 mm, respectively and openness of the exhaust valve from 2-8 mm for the corresponding flow performance is shown to be set up in Fig. 2. Table 1 shows the geometrical parameters of analyzed ports for curvatures, valve seat diameters and valve lifts (Manimaran and Senthilkumar, 2016; Salehifar *et al*., 2016; Tauro, 2016; Ren *et al*., 2016; Zhou *et al*., 2016; Sampaio and Garcia, 2016; Ervin *et al*., 2016; Sunderland *et al*., 2016).

Figure 3 is related to the analysis model configured with a finite element model for the flow analysis. Here, the model is composed of 109.960 nodes and 580.026 elements. Figure 4 represents analysis conditions for the analysis model, showing flow directions of air using arrows. As long as the analysis model of this study is realized in the combustion chamber of high temperature and high pressure rather than in the atmosphere, the pressure differences between inlet and outlet have to be large for the analysis conditions. As the analysis conditions, the exhaust gas was set up at 750°C and the difference in pressures between inside and outside of the combustion chamber at 3733 Pa

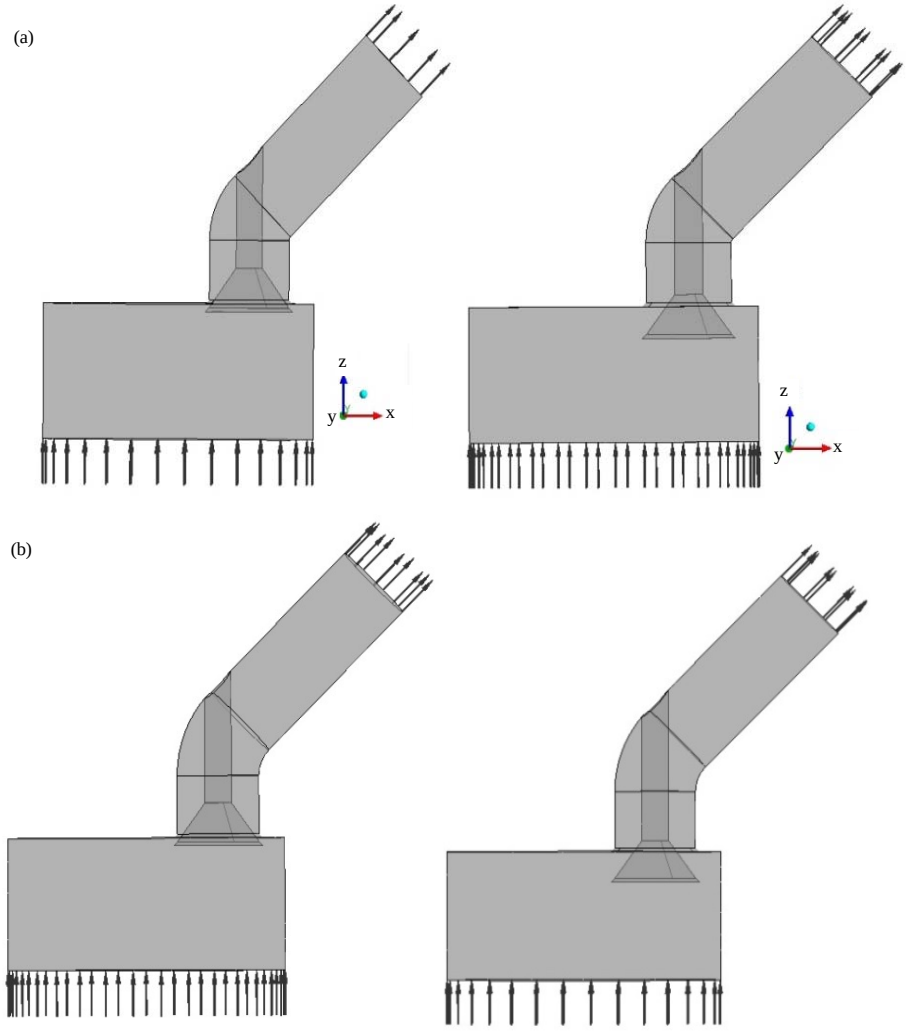

Fig. 3: Constraint conditions: a) Model 1 (R =12 mm, L: opening and closing 2 mm, R: opening and closing 8 mm and b) Model 2

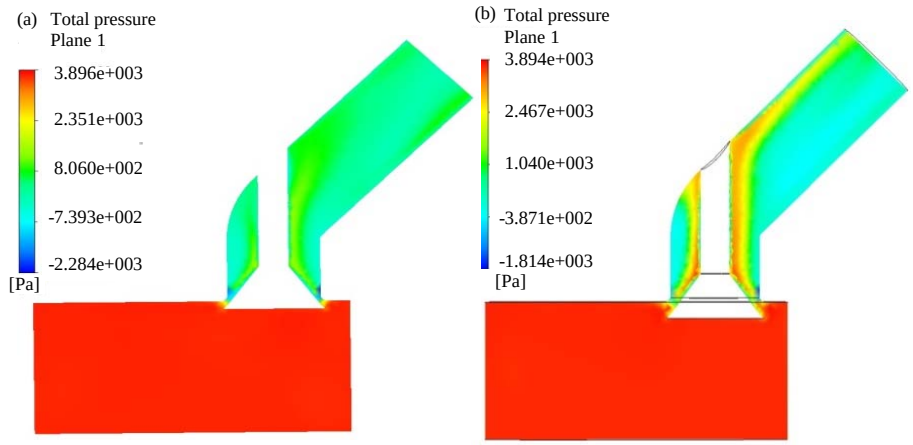

Fig. 4: Continue

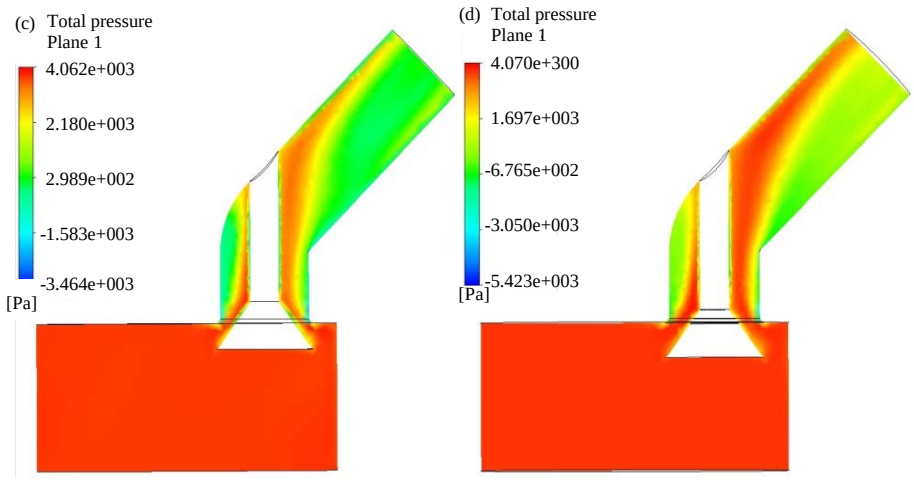

Fig. 4: Results of R = 12 mm model, total pressure: a) R12 mm, valve lift 2 mm; b) R12 mm. Valve lift 4 mm c) R12 mm, valve lift 6 mm and d) R12 mm, valve lift 8 mm

to conduct the analysis by assuming the time when gasoline was burned in the combustion chamber.

RESULTS AND DISCUSSION

Figure 4 shows the total pressure of R12 mm model. First, shows the pressure when the valve lift value is 2 mm. It can be affirmed that the pressure of cylinder part is highest and high pressures are distributed along the valve face and the stem shows the pressure when the valve lift value is 4 mm. Pressure distribution can be affirmed along the top face of exhaust port past the valve face and the stem. While the pressure distribution is similar to that when the valve lift value is 2 mm an increase in the pressure values can be affirmed shows the pressure when the valve lift value is 6 mm. Unlike the cases of and the pressure distribution became somewhat wider and slightly moved in the direction of bottom face of the exhaust port. And an increase in the pressure values can be ascertained shows the pressure when the valve lift value is 8 mm. The maximum pressure is slightly increased compared with the case of 6 mm in the valve lift value. And, the pressure distribution can be seen to have moved much toward the bottom face of exhaust port. The pressure is observed to be dropped to a negative value while passing the bottom face of exhaust port which may be considered to be an effect due to flow separation.

Figure 5 shows total pressure of R20 mm. First, shows the pressure distribution for the case where the valve lift value is 2 mm. The pressure distribution can be seen to flow along the valve seat, the valve face and the stem. When the valve lift value is 2 mm, the pressure distribution is shown to be similar to that of Fig. 5 for the exhaust port curvature of R12 mm and the valve lift of 2 mm shows the pressure distribution when the valve lift is 4 mm. The pressure can be seen to flow past the valve seat, the valve face and the stem to the rear of exhaust port. This also exhibits a s pressure distribution similar to that for the exhaust port curvature of R20 and the valve lift of 4 mm shows the pressure distribution when the valve lift is 6 mm. The pressure distribution shows very similar results when compared with Fig. 4. Namely, all of and are showing a similar appearance for the pressure distribution to that for R12 mm. However, the pressure distribution for R12 mm exhaust port shows a tendency where the pressure around the maximum pressure distribution is drastically lowered. On the other and the relatively high pressures are being maintained in the pressure distribution for R20 mm exhaust port even when some deviations occur from the maximum pressure distribution. Namely, R20 mm exhaust port shows an even pressure distribution as a whole shows the pressure distribution when the valve lift is 8 mm. The appearance can be observed where the pressure distribution was shifted much to the bottom of exhaust port. Overall shape of pressure distribution can also be seen to be similar to that for the model of exhaust port curvature being R12 mm. However, a stark difference exists when passing the bottom of exhaust port. While the flow separation can be affirmed in the valve lift of 8 mm of Fig. 4, the flow separation phenomenon is not clearly visible in the valve lift 8 mm of Fig. 5. And considering that the pressure at the bottom of exhaust port is also maintained at a positive value raher than a negative value, flowing of the flow may be considered to be smoother.

Figure 6 shows the velocity distribution of R12 mm model. First, shows the velocity distribution when the valve lift is 2 mm. Somewhat high velocities are shown

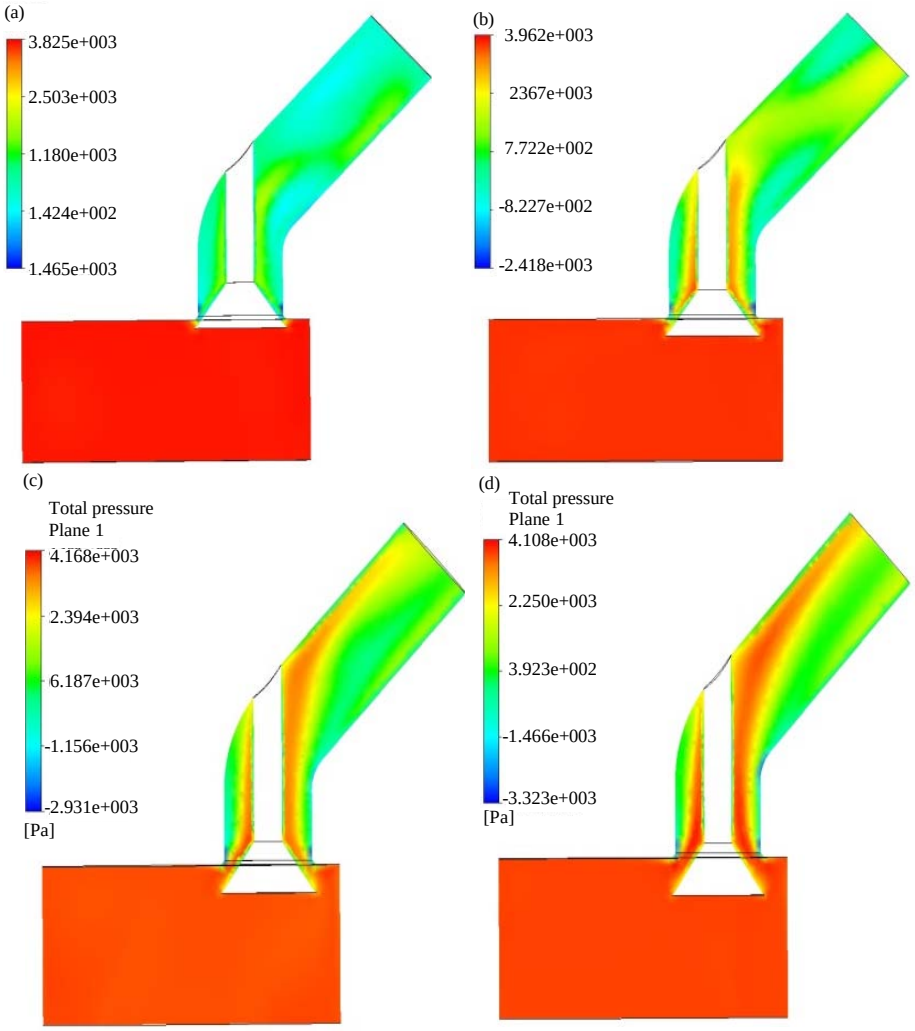

Fig. 5: Results of R = 20 mm model, total pressure: a) R20 mm, valve lift 2 mm; b) R20 mm valve lift 4 mm; c) R20 mm, valve lift 6 mm and d) R20 mm, valve lift 8mm

near the valve face and the stem part while generally even velocity distribution is exhibited otherwise shows the velocity distribution when the valve lift is 4 mm. High velocity distribution is observed up to the top face part of exhaust port past the valve face and the stem shows the velocity distribution when the valve lift is 6 mm. The appearance can be observed where the velocity distribution is much biased to the bottom face of exhaust port. However, a still even velocity distribution is shown around the valve face and the valve stem at the center shows the velocity distribution when the valve lift is 8 mm. The velocity distribution can be affirmed to be much biased to the bottom face of exhaust valve. And there exists a part where the velocity is reduced while passing through the bottom face. This may be considered as a phenomenon produced by Eddy currents due to flow separation.

Figure 7 shows velocity distribution of R20 mm model. First, shows the velocity distribution when the valve lift is 2 mm. High flow rates near the valve stem are observed and a constant appearance as whole is shown in the rear of exhaust port shows the velocity distribution when the valve lift is 4 mm. Although, high flow rates are observed near the valve stem in the same way as with the velocities are being increased shows the velocity distribution when the valve lift is 6 mm. As compared with and the maximum velocity distribution exhibits an appearance with much bias toward the bottom face of exhaust port. However, almost no phenomenon of flow separation is visible shows the velocity distribution when the valve lift is 8 mm. Although, the maximum velocity distribution shows an appearance of having been moved much toward the bottom face of the valve, the velocity drop phenomenon due to Eddy currents as the feature of

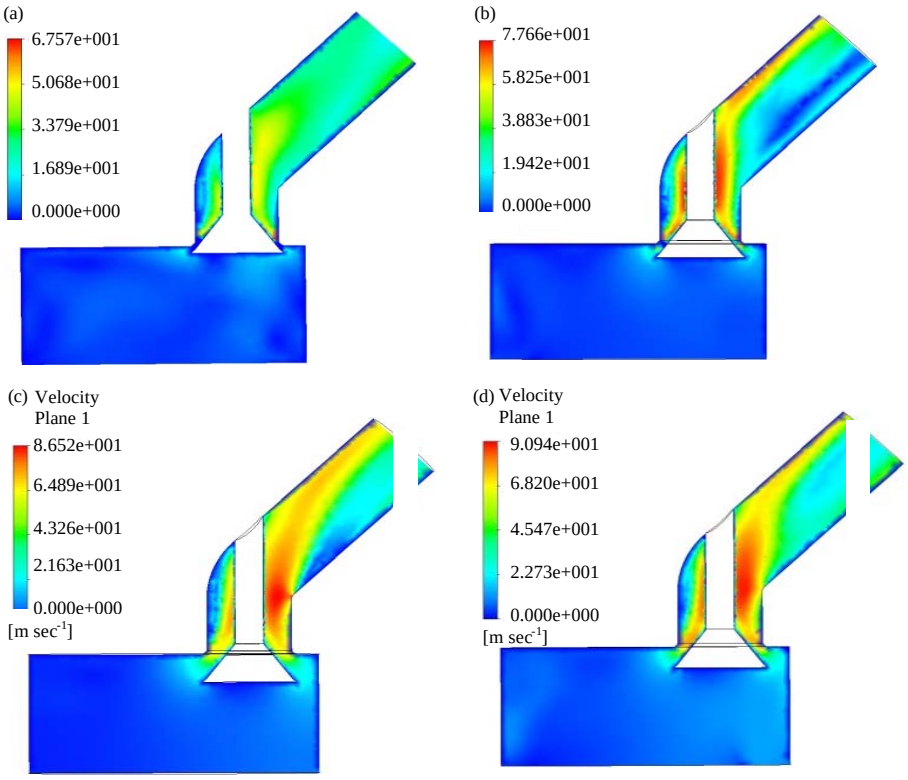

Fig. 6: Results of R = 12 mm model, fluid velocity: a) R12 mm, valve lift 2 mm; b) R12 mm. Valve lift 4 mm; c) R12 mm, valve lift 6 mm and d) R12 mm, valve lift 8 mm

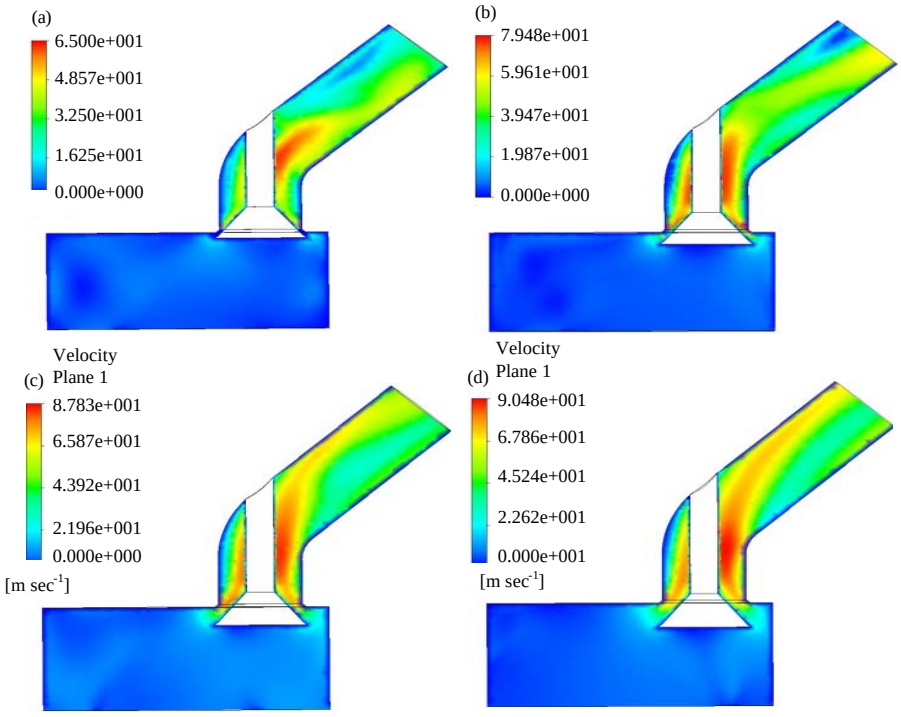

Fig. 7: Results of R = 20 mm model, fluid velocity: a) R20 mm, valve lift 2 mm; b) R20 mm. Valve lift 4 mm; c) R20 mm, valve lift 6 mm and d) R20 mm, valve lift 8 mm

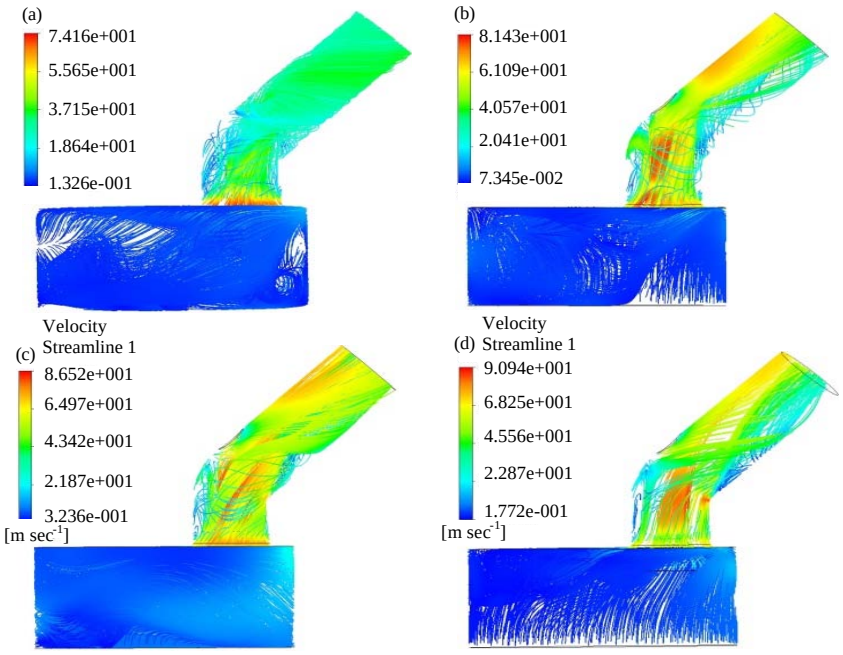

Fig. 8: Results of R = 12 mm model, fluid streamline: a) R12 mm, valve lift 2 mm; b) R12 mm. Valve lift 4 mm; c) R12 mm, valve lift 6 mm and d) R12 mm, valve lift 8 mm

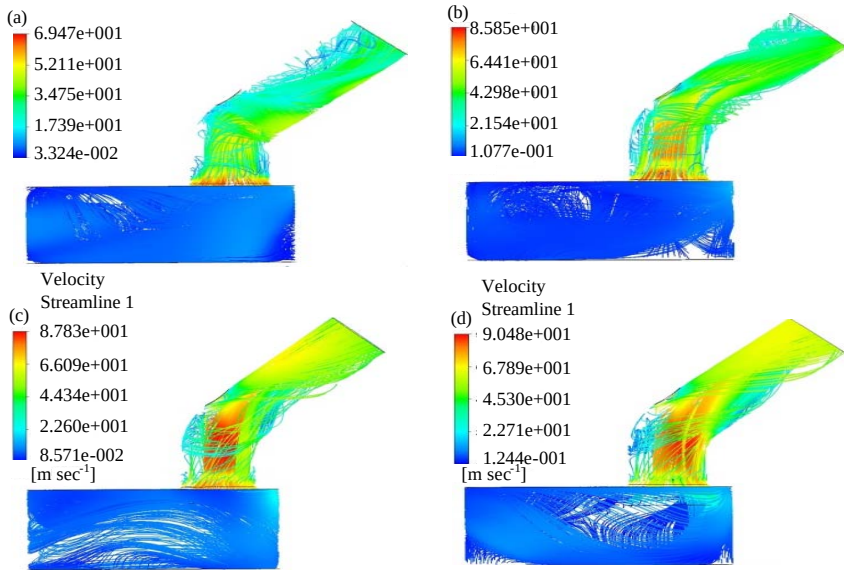

Fig. 9: Results of R = 20 mm model fluid streamline: a) R20 mm, valve lift 2 mm; b) R20 mm. Valve lift 4 mm; c) R20 mm, valve lift 6 mm and d) R20 mm, valve lift 8 mm

flow separation phenomenon is almost not visible. This is a phenomenon in much contrast to of Fig. 6. Namely, a difference in velocity difference can be seen to be clearly revealed when the valve lift value is large, although, a change in the curvature of exhaust port does not have a large effect when the valve lift value is small.

Figure 8 and 9 show velocity streamlines for R = 12 and R = 20 mm, respectively. Being velocity streamlines, shapes similar to the velocity distributions of Fig. 6 and 7 are observed. Since, the experimental conditions involve a steady flow, all of streamlines and path lines can be considered to be in agreement. Therefore, since, the

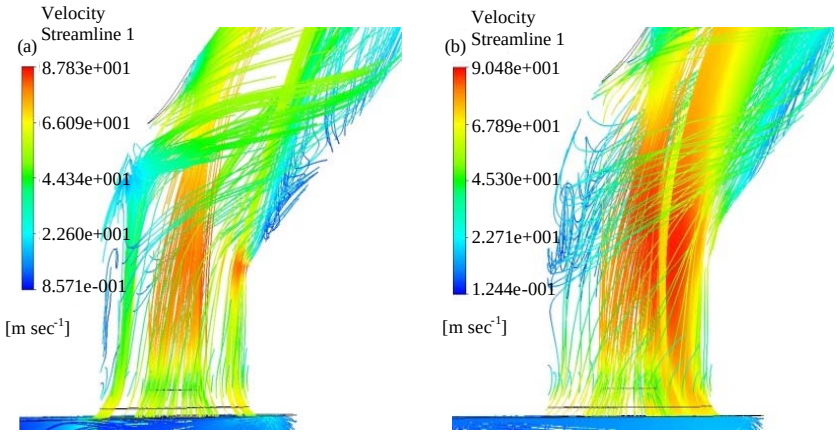

Fig. 10: Results of R = 12 mm (a) R = 20, mm and (b) model, fluid streamline: a) R12 mm, valve lift 8 mm; b) R20 mm valve lift 8 mm

streamlines of analysis results may be viewed as pursuing and visualizing the actual trajectory for motion of some fluid particle, it may be considered as a Lagrange concept. In particular, the difference is displayed more evidently at the time when the valve lift value appearing as the greatest feature in this study is large. Figure 10 magnifies Fig. 8d and 9d as the characteristic parts.

Figure 10 magnifies only the exhaust port parts among streamlines for valve lift of 8 mm in the R12 mm and R20 mm models. Although, high velocities are observed along the valve face and the valve stem as well as the top face of exhaust port when the valve lift value is small, high velocities are exhibited on the bottom face of exhaust port when the valve lift value is large. And since, the steady-state streamline may be considered to have displayed the motion trajectories of individual articles, Eddy currents and flow separation, etc. of the fluid can be seen more readily.

CONCLUSION

In this study, the improvement of flow performance as a function of diameter and curvature of the exhaust port for exhaust gas from the combustion chamber were investigated and the following conclusions have been drawn through an analysis study.

Since, the increase in diameter and curvature of combustion chamber interior under discharge environments for exhaust gas can increase the pressure differences between the combustion chamber and the exhaust port, smooth exhausting can be realized. In such result values for the pressure differences between inside and outside of combustion chamber, the performance improved by about 2.4% at the point where the valve lift was opened at the maximum could be obtained when the diameter of exhaust port of 20 mm was compared with that of 12 mm.

Here, in the result values for differences in velocities for the discharge of exhaust gas, the performance improved by about 0.5% at the point where the valve lift was opened at the maximum could be observed when the diameter of exhaust port of 20 mm was compared with that of 12 mm. Also, in the case of a large valve lift, the flow characteristics are suggested to be controlled by the port's own shape rather than that of the surroundings of valve seat. Also, flow could be affirmed to occur along the bottom part of exhaust port and the shape of port's bottom face could be determined to be important when the valve lift was large.

In the occurrence of Eddy currents inside combustion chamber, it could be seen that the internal Eddy currents had been increased for the exhaust port diameter of 20 mm when compared with that of 12 mm. Thus, smooth flow of the inhaled air could be seen to occur as the residual exhaust gas of inside could be discharged to outside due to production of such Eddy currents. Also, the practical area of flow path was reduced as the phenomenon of flow separation or thick boundary layer occurred on the port's bottom face when the curvature of the port bottom face was small. However, the Eddy currents due to flow separation could be seen to be reduced, the more increased the bottom face curvature.

Based on the results of this study, the design basic data on diameter and curvature of the exhaust port interior could be provided and it is considered that contributions can be made to optimization design.

REFERENCES

Creamers, E.M.P., 2017. Implementation of erythroid lineage analysis by flow cytometry in diagnostic models for myelodysplastic syndromes. Haematologica, 102: 320-326.

Eckhardt, J., 2017. The inverse spectral transform for the conservative Camassa-Holm flow with decaying initial data. Arch. Ration. Mech. Anal., 224: 21-52.

Ervin, V.J., H. Lee and A.J. Salgado, 2016. Generalized Newtonian fluid flow through a porous medium. J. Math. Anal. Appl., 433: 603-621.

Han, D., A. Brylev, X. Yang and Z. Tan, 2017. Numerical analysis of second order, fully discrete energy stable schemes for phase field models of two-phase incompressible flows. J. Sci. Comput., 70: 965-989.

Kim, M., S.M. Lee, D.W. Lee, S. Park and S. Kim, 2017. Tribological effects of a rough surface bearing using an average flow analysis with a contact model of asperities. Intl. J. Precis. Eng. Manuf., 18: 99-107.

Manimaran, R. and R. Senthilkumar, 2016. Performance analysis of solar water heater at possible flow rates with and without phase change material. Distrib. Gener. Altern. Energy J., 31: 67-80.

Ren, Z., W. Li, R. Billinton and W. Yan, 2016. Probabilistic power flow analysis based on the stochastic response surface method. IEEE. Trans. Power Syst., 31: 2307-2315.

Rotaru, A., 2017. Thermal and kinetic study of hexagonal boric acid versus triclinic boric acid in air flow. J. Therm. Anal. Calorim., 127: 755-763.

Salehifar, M., M. Tahani, M. Hojaji and A. Dartoomian, 2016. CFD modeling for flow field characterization and performance analysis of HGITVC. Appl. Therm. Eng., 103: 291-304.

Sampaio, L. and A. Garcia, 2016. Exploring context-sensitive data flow analysis for early vulnerability detection. J. Syst. Software, 113: 337-361.

Shaidarova, L.G., I.A. Chelnokova, M.A. Il'ina, A.V. Gedmina and H.C. Budnikov, 2017. Amperometric detection of hydroxypurines at an electrode modified with a composite based on mixed-valence ruthenium and cobalt oxides in flow injection analysis. J. Anal. Chem., 72: 107-112.

Sourdis, C., 2015. Analysis of an irregular boundary layer behavior for the steady state flow of a Boussinesq fluid. Discrete Continuous Dyn. Syst., 37: 1039-1060.

Sunderland, K., M. Coppo, M. Conlon and R. Turri, 2016. A correction current injection method for power flow analysis of unbalanced multiple-grounded 4-wire distribution networks. Electric. Power Syst. Res., 132: 30-38.

Tauro, F., 2016. Particle tracers and image analysis for surface flow observations. Wiley Interdiscip. Rev. Water, 3: 25-39.

Zhou, X., Y. Hu and J. Wang, 2016. Experimental analysis on flow past circular cylinder attached to frontal splitter plate. J. Beijing Univ. Aeronaut. Astronautics, 42: 172-179.